Vibrational Bound States of the He₂Ne⁺ Cation[†]

José Zúniga,*,[‡] Adolfo Bastida,*,[‡] Alberto Requena,*,[‡] Nadine Halberstadt,*,[§] J. Alberto Beswick,*,[§] and Kenneth C. Janda*, I

Departamento de Química Física, Universidad de Murcia, 3010 Murcia, Spain, Laboratoire Collisions, Agrégats, Réactivité, IRSAMC, Université de Toulouse, UPS, and CNRS, UMR5589, F-31062 Toulouse, France, and Department of Chemistry and Institute of Surface and Interface Science, University of California at Irvine, Irvine, California 92697-2025

Received: May 29, 2009; Revised Manuscript Received: September 4, 2009

The vibrational bound states of the He_2Ne^+ complex have been determined using a potential energy surface previously published by Seong et al. [*J. Chem. Phys.* **2004**, *120*, 7456]. The calculation was performed by sequential diagonalization—truncation techniques in a discrete variable representation using Radau hyperspherical coordinates. There are 52 bound levels. The ground state has an energy of 605.3 cm⁻¹ above the absolute minimum and lies about half way to dissociation. The evaporation energy of one He atom is equal to 866.1 cm⁻¹. Only four levels have energies below the classical energy for dissociation, and all the other 48 states are bound by the zero-point energy of the HeNe^+ fragment. The implications of the properties of the eigenvalue spectrum and of the corresponding wave functions on the vibrational relaxation dynamics and infrared spectra of He_NNe^+ clusters is discussed.

Introduction

The $\text{He}_N D^+$ cluster ions, where D is an atomic or molecular dopant, are very interesting because they represent a simple example of gas phase "solvation" of an ion, and they are amenable to experimental study. They also constitute ideal model systems for dynamical studies in a novel medium, helium nanodroplets, which provide a homogeneous, superfluid, and extremely cold environment for spectroscopic and dynamical studies of molecular species. The final stage of many experiments is the electron-impact ionization of the doped cluster. This leads to a violent fragmentation of the droplet and a distribution of $\text{He}_N D^+$, $n \ll N$, that is surprisingly difficult to predict even in the relatively simple case where the dopant is a single rare gas atom.¹⁻⁵ The relative stability of small mixed rare gas cluster ions of the type $\text{He}_n \text{Rg}^+$ has been examined by Murrell et al.,⁶ Seong et al.,⁷ and Brindle et al.⁸

The first element of this series, HeNe^+ , has been extensively studied because of its relevance to the Ne^+ ion mobility in helium. Its electronic structure is particularly interesting since the ionization energy of helium is only 2.99 eV higher than that of neon. This difference is small enough to induce a partial delocalization of the charge from the neon to the helium atom, resulting in weak covalent bonding. For instance, with the potentials used in the present work the $(\text{He}-\text{Ne})^+$ dissociation energy is $D_e = 0.669 \text{ eV} (5397 \text{ cm}^{-1})$. Unexpectedly, the mass spectra of the He_NNe^+ species do not show any structure, whereas the helium and argon ones do. Diffusion Monte Carlo simulations have shown that this absence of shell structure is due to important zero-point effects resulting in very diffuse wave

functions and a smooth variation of the incremental bonding energy with the number of helium atoms.

The ion is also very interesting. It is the ionic core in the He_NNe^+ series, the additional helium atoms being mainly bound by electrostatic interaction to this core. Its second helium is bound by 0.127 eV (1026 cm⁻¹). This value is relatively large relative to pure electrostatic bonding and may be at least partially responsible for the fact that fragments are more prevalent in experimental data than in ref 8.

Ab initio calculations of Seong et al.⁷ for the He₂Ne⁺ complex have yielded an asymmetric collinear (He–Ne–He)⁺ geometry with a small barrier between two equivalent minima. Because of its practical interest, as well as its peculiar potential energy surface, we have undertaken a study of its bound states which could be useful for experiments trying to identify its presence or its vibrational relaxation rates. Vibrational relaxation is expected to play an important role in the dissociation of helium droplets once the charge has been localized on the neon atom, and the two main candidates to relax energy are HeNe⁺ and He₂Ne⁺.

In this paper, we present the calculation of all vibrational states of the ${\rm He_2Ne^+}$ complex for total angular momentum zero. The theoretical treatment of these types of wide amplitude floppy systems relies heavily on the choice of internal coordinates. Orthogonal coordinates are particularly useful because the kinetic energy operators are easy to evaluate, and this facilitates the calculation of the corresponding differential matrix elements. This issue has been discussed in great detail by Aquilanti and co-workers. $^{10-13}$ The hyperspherical versions of these coordinates are particularly interesting for systems such as ${\rm He_2Ne^+}$ with two identical light atoms and a third heavier atom. In this work we have used Radau hyperspherical coordinates.

The potential energy surface is given by a diatomics-inmolecule (DIM) model based on ab initio calculations for He₂Ne⁺ and the best available potentials for He₂ and HeNe dimers, as discussed in detail in ref 7. This potential has been previously used for diffusion Monte Carlo calculations of

[†] Part of the "Vincenzo Aquilanti Festschrift".

^{*} To whom correspondence should be addressed. E-mail: zuniga@um.es; bastida@um.es; requena@um.es; nhalbers@irsamc.ups-tlse.fr; beswick@irsamc.ups-tlse.fr; kcjanda@uci.edu.

^{*} Universidad de Murcia.

[§] Université de Toulouse.

[&]quot;University of California at Irvine.

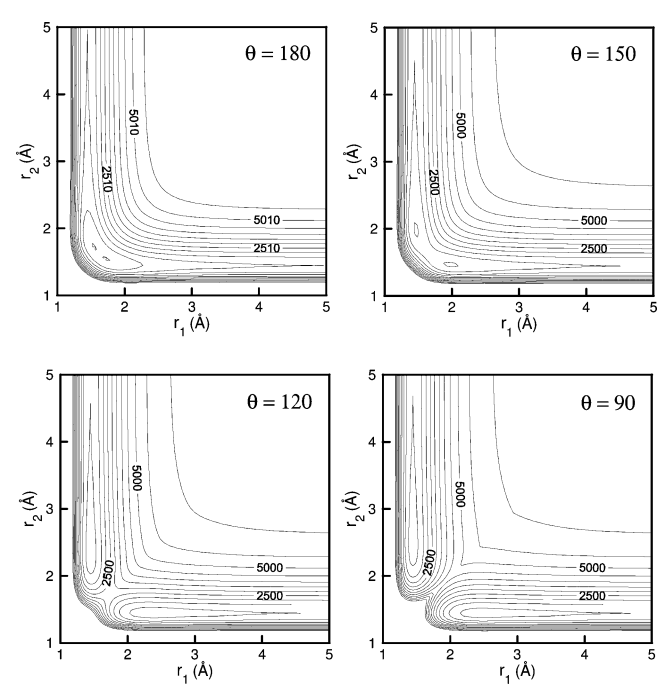


Figure 1. Contour plots of the DIM potential energy surface of the He_2Ne^+ complex in internal coordinates at the colinear $\theta=180^\circ$ and bent $\theta=150^\circ$, 120° , and 90° geometries. Contours are spaced by 500 cm^{-1} , the lowest-energy contour being at 500 cm^{-1} . The zero of energy is chosen at the potential minimum.

He_NNe⁺ cluster stabilities.⁸ The detailed description of the potential energy surface is presented here for completeness.

The vibrational states with no rotation have been calculated using sequential diagonalizations and truncations in a discrete variable representation (DVR) (with hyperspherical Radau coordinates). The resulting eigenvalues and wave functions are discussed and analyzed.

Potential Energy Surface

The potential energy surface is very similar to that previously reported by by Seong et al.⁷ using the diatomics-in-molecule (DIM) method. In Figure 1, contour plots in internal bond coordinates are presented for different values of the bending angle θ . As borne out by the most recent ab initio calculations,^{7,14} the equilibrium geometry is colinear and asymmetric (He-Ne-He)⁺ (see Figure 1) with two minima corresponding to one bond length of 1.55 Å and the other one of 1.72 Å. The barrier between the two minima is at $r_1 = r_2 = 1.62$ Å with a height of 0.0018 eV (14.59 cm⁻¹). Note that these values are slightly different from those presented in ref 4 due to an error in the program which has now been corrected. The bonding energy is $D_e = 0.796384$ eV (6423.28 cm⁻¹) with $D_e = IE(\text{He}_2\text{Ne}^+) - 2E(\text{He}) - E(\text{Ne}^+)$, and the classical dissociation energy for one He atom elimination is 0.127193 eV (1025.88 cm⁻¹).

Away from the colinear configuration ($\theta=180^\circ$), the height of the barrier separating the two equivalent minima increases. This is apparent in Figure 1 where contour plots of the potential for $\theta=150^\circ$, 120° , and 90° are presented (the barrier for $\theta=90^\circ$ is between the 4500 and 5000 cm⁻¹ equipotentials). Figure 2 presents the variation of the potential energy along the minimum energy path going from the equilibrium colinear configuration (He–Ne–He)⁺ ($\theta=180^\circ$) to the colinear asymmetric (He–He–Ne) ⁺ ($\theta=0^\circ$) configuration. As observed in this figure, the potential function has also a very

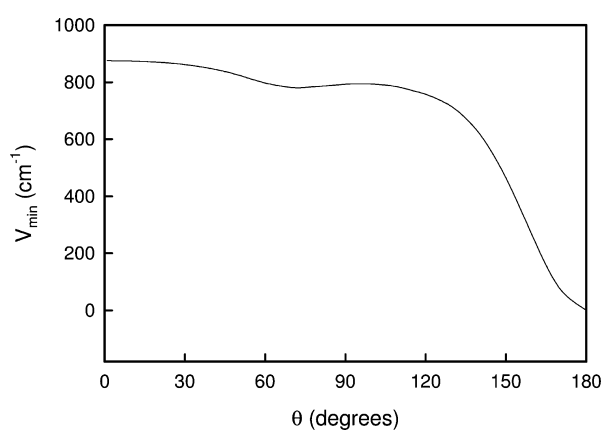


Figure 2. Minimum energy path of the DIM potential energy surface of the He_2Ne^+ complex as a function of the valence angle θ . The zero of energy is chosen at the potential minimum.

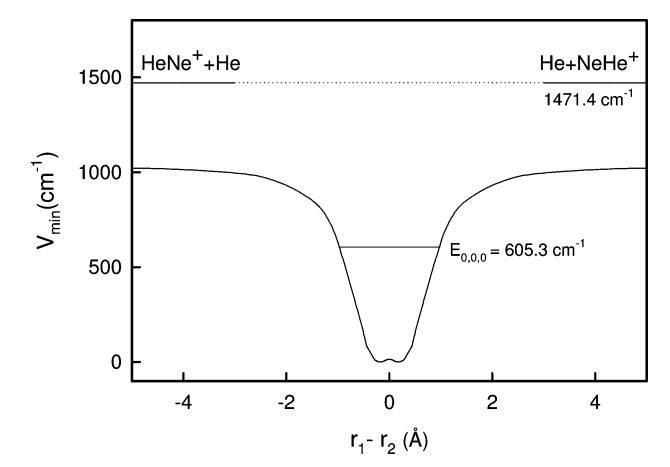


Figure 3. Minimum energy path of the DIM potential energy surface of the He_2Ne^+ complex as a function of the difference $r_1 - r_2$ of bond lengths in the colinear geometry ($\theta = 180^\circ$). The zero of energy is chosen at the potential minimum, and the horizontal line includes the zero-point energy of the HeNe^+ fragment. Also shown is the ground energy level of the He_2Ne^+ complex, labeled $E_{0.0.0}$.

shallow local minimum (\approx 13 cm⁻¹) at r_1 = 1.44 Å, r_2 = 2.54 Å, and θ = 72°.

We have also represented the minimum energy path associated with the asymmetric bond coordinate r_1-r_2 for the colinear configuration $\theta=180^\circ$ (Figure 3) and for the bent geometries $\theta=150^\circ$ and $\theta=120^\circ$ (Figure 4). These figures clearly show how the potential barrier between the two equivalent minima increases and the well depth of these minima decreases as the molecule bends. It is expected that this strong θ dependence of the potential energy surface will have a profound effect on the structure of the vibrational energy levels (see below).

That the He₂Ne⁺ potential energy surface calculations are very sensitive to the basis set and correlation method employed was discussed in some detail in ref 7. That study focused on the details of the potential energy minima and the barrier between them. For the CCSD(T) method using a triple- ζ basis set with full counter poise, CP, correction, the two bond lengths were found to be 1.50 and 1.85 Å, compared to 1.52 and 1.72 Å using the DIM method employed here. The total binding energy was found to be 0.61 eV using the triple- ζ basis with CP correction: this increased to 0.717 eV using quadruple- ζ but no CP correction. These numbers compare to 0.796 eV for the DIM potential. Finally, the transition state between the minima has symmetric bond lengths of 1.63 Å, triple- ζ , and 1.62 Å, DIM. The barrier height is 0.1 eV, triple- ζ , 0.007 eV, quadruple-

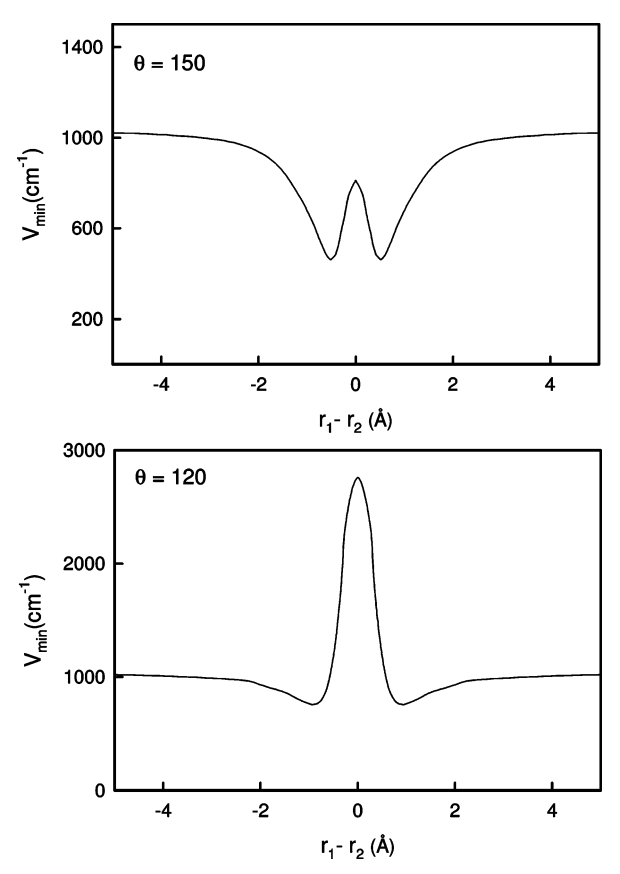


Figure 4. Minimum energy path of the DIM potential energy surface of the He_2Ne^+ complex as a function of the difference r_1-r_2 of bond lengths in the bent $\theta=150^\circ$ (b) and $\theta=120^\circ$ (c) geometries. The zero of energy is chosen at the potential minimum.

 ξ , and 0.0018 DIM. So, the DIM potential slightly overestimates the total bond energy, resulting in a shorter bond for the more weakly bonded helium atom, and underestimates the barrier height at the transition state. Note, however, that these differences are quite small with respect to the zero-point energy of the ground vibrational state, reported later. Also, we have considerable confidence in the portions of the potential energy surface away from the potential minima since these are based on diatomic potential energy curves that have been tested against scattering and spectroscopy, as discussed in ref 7. We expect that the essential features of the nuclear wave functions reported below will survive future improvements in the potential energy surface determination.

Methodology for the Calculation of Vibrational Bound States

To calculate all the vibrational bound states of the He₂Ne⁺ complex, we have used a truncation—diagonalization method based on discrete variable representation (DVR) basis functions. These methods are currently routinely used to compute energy eigenvalues and wave functions of floppy triatomic molecules which undergo very large-amplitude vibrational motions, as can be expected for a system such as He₂Ne⁺. In this work, we use these techniques to construct compact basis functions expressed as linear combinations of DVR functions, as developed by Light and co-workers^{16,24,25} and by Tennyson and co-workers. The compact basis functions expressed as linear combinations of DVR functions, as developed by Light and co-workers^{16,24,25} and by Tennyson and co-workers.

The DVR-based methods are most conveniently used in conjunction with orthogonal coordinates due to the simple form of the kinetic energy operators, which facilitates the calculation of the corresponding differential matrix elements. In this work, we have used Radau hyperspherical coordinates to calculate the vibrational bound states of He_2Ne^+ . These coordinates are defined as follows^{27,28}

$$\rho = \sqrt{s_1^2 + s_2^2} \tag{1}$$

$$\phi = \arctan\left(\frac{s_2}{s_1}\right) \tag{2}$$

$$\theta = \arccos\left(\frac{\mathbf{s}_1 \mathbf{s}_2}{s_1 s_2}\right) \tag{3}$$

where \mathbf{s}_1 and \mathbf{s}_2 are the mass-scaled Radau vectors which join the so-called canonical point of the molecule with the end atoms. ^{29,30} The (pure) vibrational ($\mathbf{J}=0$) Hamiltonian of the triatomic ABC molecule for these coordinates can be expressed in the form²⁸

$$\hat{H}(\rho,\phi,\theta) = -\frac{\hbar^2}{2\mu} \left[\frac{\partial^2}{\partial \rho^2} + \frac{1}{4\rho^2} + \frac{1}{\rho^2} \frac{\partial^2}{\partial \phi^2} + \frac{1}{\rho^2 \sin^2 \phi \cos^2 \phi} \frac{1}{\sin \theta} \frac{\partial}{\partial \theta} \sin \theta \frac{\partial}{\partial \theta} \right] + V(\rho,\phi,\theta) \quad (4)$$

where $\mu = (m_{\rm B}(m_{\rm A}m_{\rm C})^{1/3}/M)^{3/2}$; $M = m_{\rm A} + m_{\rm B} + m_{\rm C}$; and the volume element is given by $d\tau = d\rho d\phi d\theta \sin \theta$.

The first step in the successive truncation—diagonalization method is the determination of the primitive DVR basis function sets. These sets are obtained by diagonalizing the matrix of each hyperspherical coordinate in a finite basis representation (FBR), namely $\{F_l(\rho)\}$, $\{F'_m(\phi)\}$, and $\{F''_n(\theta)\}$. The hyperspherical DVR functions $\{D_{\rho_l}(\rho)\}$, $\{D'_{\phi_l}(\phi)\}$, and $\{D''_{\theta_k}(\theta)\}$ are related to the FBR functions by

$$D_{\rho_i}(\rho) = \sum_{l=1}^{N_{\rho}} R_{li} F_l(\rho) \tag{5}$$

$$D'_{\phi_j}(\phi) = \sum_{m=1}^{N_{\phi}} R'_{mj} F'_m(\phi)$$
 (6)

$$D''_{\theta_k}(\theta) = \sum_{n=1}^{N_{\theta}} R''_{nk} F''_{n}(\theta)$$
 (7)

The FBR functions used in this work are particle-in-a-box functions for ρ and ϕ and Legendre polynomials for the bending angle θ

The second step of the method consists of determining the two-dimensional (2D) contracted DVR basis set to be used in the diagonalization of the total Hamiltonian matrix. The vibrational coordinate that naturally defines the 2D basis set is, in this case, the angle θ . Accordingly, we solve first the 2D eigenvalue equation for the hyperspherical coordinates ρ and ϕ with θ frozen at the discrete DVR points θ_k . The 2D eigenvalue equation is then

$$\label{eq:continuous_equation} \begin{split} \left[-\frac{\hbar^2}{2\mu} \left(\frac{\partial^2}{\partial \rho^2} + \frac{1}{4\rho^2} + \frac{1}{\rho^2} \frac{\partial^2}{\partial \phi^2} \right) + V(\rho, \phi, \theta_k) \right] \psi_{n\theta_k}^{\text{2D}}(\rho, \phi) &= \\ E_{n\theta_k}^{\text{2D}} \psi_{n\theta_k}^{\text{2D}}(\rho, \phi) \quad (8) \end{split}$$

It is solved by expressing the 2D wave functions $\psi_{n\theta_k}^{\text{2D}}(\rho, \phi)$ as linear combinations of the direct product of DVR basis functions $D_{\rho_i}D'_{\phi_i}$, i.e.

$$\psi_{n\theta_{k}}^{2D}(\rho,\phi) = \sum_{i=1}^{N_{\rho}} \sum_{i=1}^{N_{\phi}} C_{i,j,n,\theta_{k}}^{2D} D_{\rho_{i}}(\rho) D'_{\phi_{j}}(\phi)$$
(9)

For each discrete value of the angle θ_k , this expansion is truncated by retaining only those DVR-product basis functions which satisfy the condition¹⁶

$$V(\rho_i, \phi_i, \theta_k) < V_{\text{max}} \tag{10}$$

where $V_{\rm max}$ is a given potential energy cutoff. Thus, we select a number $N^{2D}(\theta_k)$ of two-dimensional DVR basis functions for each angle θ_k . The energies $E^{\rm 2D}_{n\theta_k}$ and the expansion coefficients $C^{\rm 2D}_{i,j,n,\theta_k}$ of the 2D wave functions $\psi^{\rm 2D}_{n\theta_k}(\rho,\phi)$ are determined by diagonalizing the corresponding DVR Hamiltonian matrices.

In the third step of the method, we proceed by expanding the three-dimensional wave functions in terms of the basis functions formed by the products of the contracted 2D functions $\psi_{n\theta_k}^{\rm 2D}(\rho,\phi)$ and the angular DVR functions D''_{θ_k} . Thus, we write

$$\psi_l^{3D}(\rho, \phi, \theta) = \sum_{k=1}^{N_{\theta}} \sum_{n=1}^{N^{2D}} C_{k,n,l}^{3D} \psi_{n\theta_k}^{2D}(\rho, \phi) D''_{\theta_k}(\theta)$$
 (11)

and the 3D Hamiltonian matrix elements are given by

$$\langle D''_{\theta_{k}} \psi_{n\theta_{k}}^{2D} | \hat{H} | D''_{\theta_{k}} \psi_{n\theta_{k}}^{2D} \rangle = E_{n\theta_{k}}^{2D} \delta_{n,n'} - \frac{\hbar^{2}}{2\mu} \langle D''_{\theta_{k}} | \frac{1}{\sin \theta} \frac{\partial}{\partial \theta} \times \sin \theta \frac{\partial}{\partial \theta} | D''_{\theta_{k}} \rangle \langle \psi_{n'\theta_{k}}^{2D} | (\rho^{2} \sin^{2} \phi \cos^{2} \phi)^{-1} | \psi_{n\theta_{k}}^{2D} \rangle + \langle D''_{\theta_{k}} \psi_{n'\theta_{k}}^{2D} | V | D''_{\theta_{k}} \psi_{n\theta_{k}}^{2D} \rangle$$
(12)

The size of the three-dimensional basis set is then $\sum_{k=1}^{N_{\theta}} N^{\text{2D}}(\theta_k)$. This basis is contracted in turn by retaining in expansion eq 11 only those functions with 2D energies $E_{n\theta_k}^{\text{2D}}$ below a second energy cutoff E_2^{cut} , that is, by imposing the condition

$$E_{n\theta_k}^{\text{2D}} < E_2^{\text{cut}} \tag{13}$$

The three-dimensional vibrational wave functions are then given by eq 11 with the double sum extended over the $N^{\rm 3D}$ pairs of indexes k and n that satisfy eq 13. The coefficients $C_{k,n,l}^{\rm 3D}$ and the energy eigenvalues are calculated by diagonalizing the three-dimensional Hamiltonian matrix.

Results and Discussion

The bound vibrational states of the He₂Ne⁺ complex have energies below 1471.42 cm⁻¹ measured from the bottom of the well. This corresponds to the energy threshold for the expulsion of the first He atom, which is the sum of the classical binding

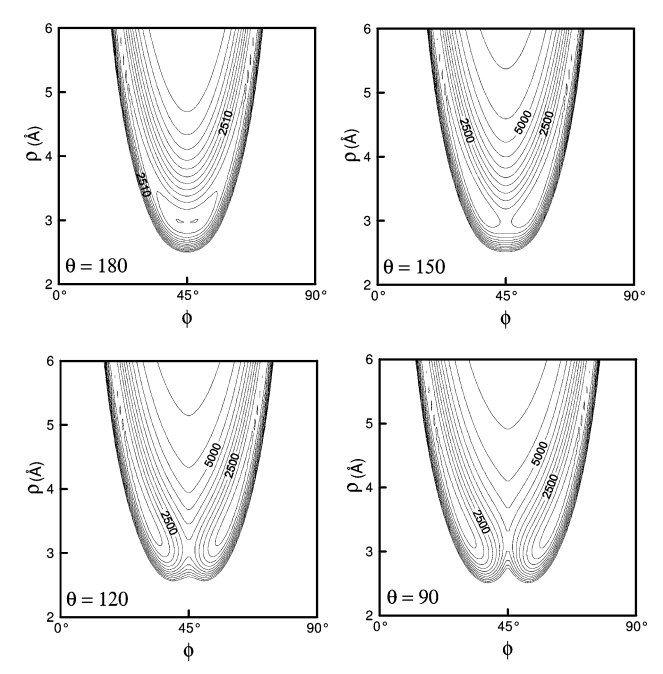


Figure 5. Contour plots of the DIM potential energy surface of the He_2Ne^+ complex in hyperpherical Radau coordinates at the colinear $\theta = 180^\circ$ and bent $\theta = 150^\circ$, 120° , and 90° geometries. Contours are spaced by 500 cm^{-1} , the lowest-energy contour being at 500 cm^{-1} . The zero of energy is chosen at the potential minimum.

energy of the He atom (1025.88 cm⁻¹) plus the vibrational energy of the ground state of HeNe⁺, $E_{v=0}$ (HeNe⁺) = 445.54 cm⁻¹³¹ (see Figure 3).

In Figure 5 we present the bidimensional contour plots of the DIM surface for He_2Ne^+ in hyperspherical Radau coordinates (ρ,ϕ) for bending angles $\theta=180^\circ,150^\circ,120^\circ,$ and $90^\circ.$ As can be seen from the figure, these contour plots allow one to fix quite naturally the limits of the quantization box providing the DVR wave functions. In fact, these limits have been taken to be the same for all values of the bending angle θ_k . The ϕ coordinate plays the role of the asymmetric mode in the limit of small amplitudes. The symmetry of the potential energy surface with respect to the maximum of the barrier (located at $\phi=45^\circ$) allows us to calculate separately the odd and even states, thus reducing the numerical effort.

We have started by setting the box limits, $\rho = [2, 6]$ Å, $\phi = [0, 90]^\circ$, and the value of the cutoff $V_{\rm max}$ for the energies of bidimensional wave functions, according to the condition in eq 10, at 6000 cm⁻¹, very near the 3-body dissociation energy of the complex ($D_{\rm e} = 6423.28~{\rm cm}^{-1}$). The number of basis functions for each coordinate has been set such that (N_{ρ} , N_{ϕ} , N_{θ}) = (160,130,30), and the second cutoff $E_{\Sigma}^{\rm cut}$ for the energies of the 3-dimensional wave functions in eq 13 has been taken as 2500 cm⁻¹, considerably above the threshold for dissociation at 1471.42 cm⁻¹. The results for the even symmetry levels are presented in the second column of Table 1. A convergence study with respect to the DVR parameters has been conducted, and the results are presented in the other columns of Table 1.

We have first increased the upper limit ρ_{max} for ρ with all the other DVR parameters fixed. Only those states very near the dissociative limit are modified. For $\rho_{max} = 14$ Å, almost all states are stabilized, and for $\rho_{max} = 18$ Å, the energy of all the states is converged to the first decimal figure. The values are given in the third column of Table 1. Using the interval [2,18] Å for the ρ coordinate, we have then increased selectively the number of basis functions for each coordinate starting from their

TABLE 1: Convergence of the Even Vibrational Energy Levels (in cm⁻¹) of He₂Ne⁺ with Respect to the Parameters of the Truncation—Diagonalization DVR Calculation

the Huncation Diagonalization DVK Calculation			
$[2,6]^a$	[2,18]	[2,18]	[2,18]
$\overline{(160,130,30)^b}$	(160,130,30)	(160,130,40)	(160,130,40)
6000°	6000	6000	6200
-2500^{d}	2500	2500	2500
605.3	605.3	605.3	605.3
919.5	919.5	919.5	919.4
992.2	992.2	992.2	992.2
1139.5	1139.4	1139.4	1139.4
1192.7	1192.7	1192.7	1192.7
1264.4	1264.3	1264.3	1264.3
1279.7	1279.7	1279.7	1279.6
1301.6	1301.6	1301.6	1301.6
1309.0	1308.9	1308.9	1308.9
1325.4	1325.4	1325.4	1325.4
1341.5	1341.5	1341.5	1341.5
1363.4	1363.4	1363.3	1362.8
1373.8	1373.8	1373.7	1373.2
1385.8	1385.8	1385.7	1384.8
1393.6	1393.5	1393.0	1389.0
1405.1	1405.0	1405.0	1404.9
1417.4	1417.2	1416.5	1411.2
1426.0	1425.7	1425.6	1425.2
1431.7	1431.0	1430.6	1428.3
1444.8	1442.5	1442.0	1437.4
1450.5	1448.6	1448.4	1445.3
1453.9	1453.1	1452.4	1449.9
1458.2	1454.5	1454.2	1452.3
1471.0	1458.4	1458.3	1457.3
1481.1	1468.6	1468.5	1466.8
1482.5	1469.4	1469.2	1467.1
1485.6	1472.3	1471.8	1468.5
			$ \begin{array}{c ccccccccccccccccccccccccccccccccccc$

 $^{^{}a}$ [ρ_{\min} , ρ_{\max}] (Å). b (N_{ρ} , N_{ϕ} , N_{θ}). c V_{\max} (cm⁻¹). d E_{2}^{cut} (cm⁻¹).

initial values $(N_{\rho}, N_{\phi}, N_{\theta}) = (160, 130, 30)$. The results show that the energies are converged with respect to N_{ρ} and N_{ϕ} , but they vary slightly, of the order of 0.5 cm⁻¹, when N_{θ} is increased up to 40. Further test calculations showed that these results are converged with respect to N_{θ} . The energy levels using $(N_{\rho}, N_{\phi}, N_{\theta}) = (160, 130, 40)$ are thus presented in the fourth column of Table 1. Finally, the convergence with respect to the cutoff energies $V_{\rm max}$ and $E_2^{\rm cut}$ has been studied. The results are unchanged when E_2^{cut} is increased, but they are still sensitive to the value of V_{max} . Starting from n = 12 they decrease by an amount of about $1-2 \text{ cm}^{-1}$ when V_{max} is increased to 6200 cm⁻¹. The results for this value of V_{max} are presented in the last column of Table 1. Additional convergence tests were performed using larger basis sets to further confirm the values given in the last column of Table 1 and in Table 2 (even and odd states) to within 0.1 cm^{-1} .

In summary, we have determined all the bound levels of the ${\rm He_2Ne^+}$ complex with a convergence in energy of the order of 0.1 cm⁻¹ using $(N_\rho,N_\phi,N_\theta)=(160,130,40)$ DVR primitive functions for each vibrational mode and cutoff energies $V_{\rm max}=6200~{\rm cm^{-1}}$ and $E_2^{\rm cut}=2500~{\rm cm^{-1}}$. These calculations have required a total of 3803 and 3788 DVR tridimensional basis functions for the even and odd parity states, respectively. We have found that there are 52 bound levels, 27 even ones, and 25 odd ones. The converged energies for both even and odd parities are collected in Table 2.

The ground state has an energy of 605.3 cm⁻¹ above the absolute minimum, and so it lies about half way to dissociation. It is interesting to note that only four levels (three even and one odd) have energies below the classical energy for dissocia-

TABLE 2: Vibrational Bound-State Energy Levels (in cm⁻¹) of the He₂Ne⁺ Complex

n	even levels	n	odd levels
1	605.3	1	763.0
2	919.4	2	1037.7
3	992.2	3	1086.8
4	1139.4	4	1211.4
5	1192.7	5	1256.9
6	1264.3	6	1296.1
7	1279.6	7	1315.9
8	1301.6	8	1333.9
9	1308.9	9	1347.2
10	1325.4	10	1362.1
11	1341.5	11	1374.8
12	1363.8	12	1382.6
13	1373.2	13	1396.3
14	1384.8	14	1404.9
15	1389.0	15	1418.5
16	1404.9	16	1422.5
17	1411.2	17	1433.9
18	1425.2	18	1437.6
19	1428.3	19	1445.5
20	1437.4	20	1450.3
21	1445.3	21	1456.7
22	1449.9	22	1461.4
23	1452.3	23	1463.6
24	1457.3	24	1468.3
25	1466.8	25	1470.7
26	1467.1		
27	1468.5		

tion (1025.9 cm $^{-1}$). All the other 48 states are bound because of the zero-point quantum energy of the HeNe $^+$ fragment which is 445.54 cm $^{-1}$. The quantum result for the evaporation energy of one He atom is then equal to 866.1 cm $^{-1}$. This value is obtained from the classical dissociation energy (1025.9 cm $^{-1}$), the HeNe $^+$ zero-point energy (445.54 cm $^{-1}$), and the energy of the He₂Ne $^+$ ground level found in this work (605.3 cm $^{-1}$).

The contour plots in (ρ, ϕ) of the probability density at the equilibrium colinear configuration are presented in Figure 6 and Figure 7 for the first six vibrational wave functions with even and odd parities, respectively. Since the barrier between the two equivalent asymmetric minima is very low $(\Delta V_b = 14.59~\text{cm}^{-1})$ as compared with the zero-point vibrational energy (605.3 cm⁻¹), it is expected that the node structure of the wave functions will be essentially the same as that of a single minimum potential. This is indeed what is observed in Figure 6 and Figure 7 for n = 1, 2, 4, 6, and the probability density at the barrier configuration $(\phi = 45^{\circ})$ is maximum for the even parity states and zero for the odd parity states.

On the other hand, for n=3 and 5 even parity states, the nodal structure is typical of a double minima potential near or just above the barrier: the maxima are localized closer to the potential wells of Figure 5, and they connect above the barrier. These states thus feel the barrier between the two equivalent minima. Since the barrier height is very small at the equilibrium colinear configuration $\theta=180^\circ$ and it increases when θ decreases, we deduce that these states correspond to a bending excitation

We now turn to the assignment of the vibrational levels. As noted before, ϕ is the antisymmetric stretch in the limit of small oscillations and ρ the symmetric stretch. By examining the nodes of the wave functions in Figure 6 and Figure 7, the first excited states with a single well pattern, ψ_1^- , ψ_2^+ , ψ_2^- , and ψ_4^+ , can be assigned to overtones in the asymmetric mode: (0,0,1), (0,0,2), (0,0,3), and (0,0,4) in the notation for triatomic vibrational levels. The wave functions ψ_6^- and ψ_6^+ have a node along the ρ

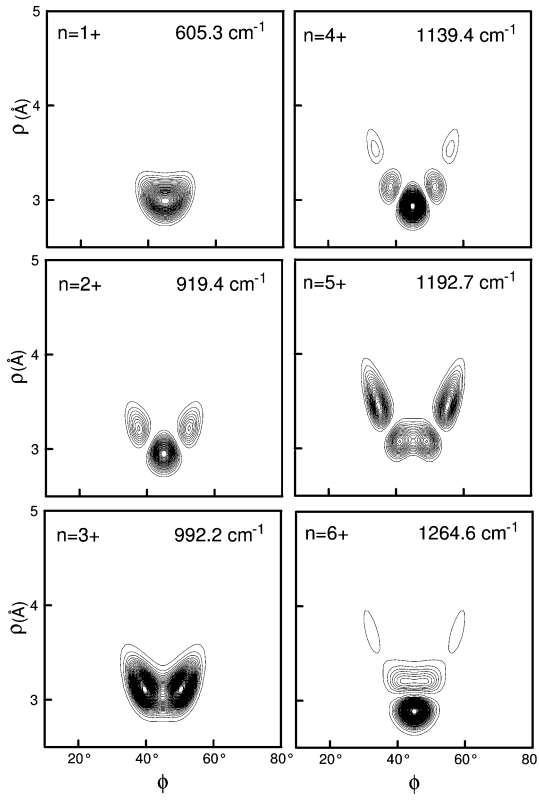


Figure 6. Contour plots of the probability density for the first six even wave funcions of He_2Ne^+ in hyperspherical Radau coordinates ρ and ϕ at the colinear ($\theta=180^\circ$) geometry.

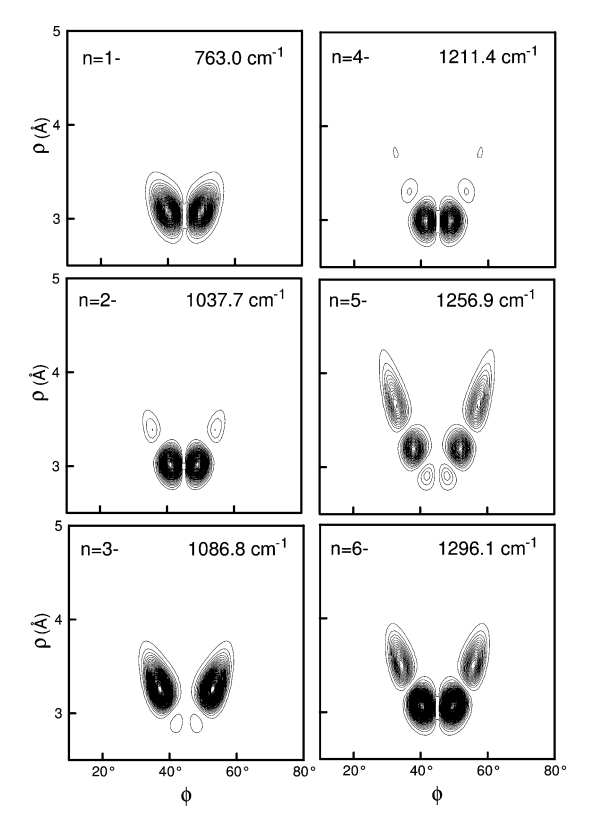


Figure 7. Same as Figure 6 for the first six odd wavefuncions (squared) of He₂Ne⁺.

coordinate and therefore can be assigned to one quantum in the symmetric stretch mode, (1,0,0) and (1,0,1), respectively. The excited states with a double well pattern, ψ_3^+ and ψ_5^+ , have a node in the θ coordinate (see Figure 8). Hence they are

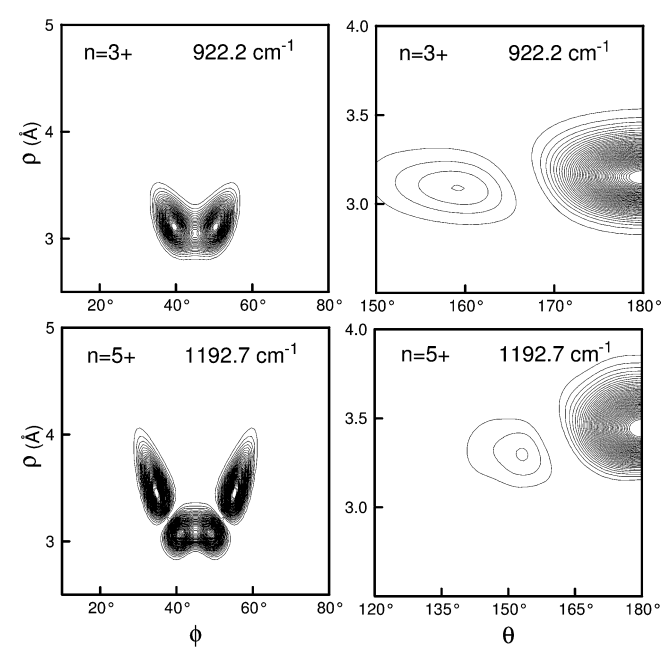


Figure 8. Contour plots of the probability density for the ψ_3^+ and ψ_5^+ states in hyperspherical Radau coordinates (ϕ, ρ) at colinear geometry (left panel) and (θ, ρ) for $\phi = 45^{\circ}$ (right panel).

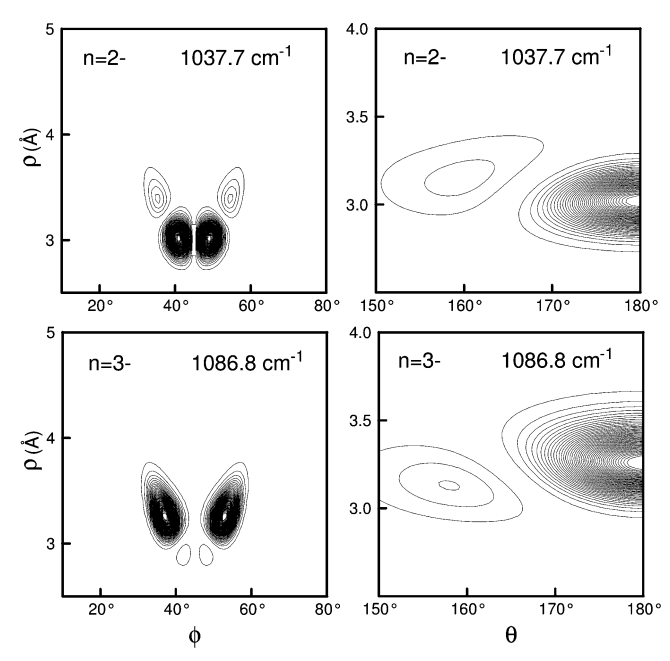


Figure 9. Same as Figure 8 for the ψ_2^- and ψ_3^- states.

assigned to (0, 2, 0) and (0, 2, 2). The ψ_3^- , ψ_4^- , and ψ_5^- states are a little less straightforward to assign, presumably because of mixing of excitations (Fermi resonances). As can be seen in Figure 9, ψ_2^- and ψ_3^- already have some bending excitation. Hence, ψ_2^- and ψ_3^- could correspond to a resonant pair (0,0,3) and (0,2,1). This is also true for ψ_4^- and ψ_5^- which can be assigned as the resonance pair (0,2,3) and (0,0,5).

All these assignments are collected in Table 3. From the first excitation in each mode, the frequencies for asymmetric stretch, bend, and symmetric stretch would be 157.7, 386.9, and 659.0 cm⁻¹, respectively. However, the asymmetric stretch frequency decreases dramatically above $v_{\rm as}=2$ because of the floppiness of the system. For the other modes, there are not enough assigned excited levels to study their frequency evolution. Indeed, the vibrational wave functions for higher excited states

TABLE 3: Vibrational Frequencies (in cm⁻¹) for the First Vibrational Bound States of the He₂Ne⁺ Complex

	-	
assignment (v_s, v_b, v_a)	frequency	energy
(0,0,0)		605.3
(0,0,1)	157.7	763.0
(0,0,2)	314.1	919.4
(0,2,0)	386.9	992.2
(0,0,3)	432.4	1037.7
(0,2,1)	481.5	1086.8
(0,0,4)	534.1	1139.4
(0,2,2)	587.4	1192.7
(0,2,3)	606.1	1211.4
(0,0,5)	651.6	1256.9
(1,0,0)	659.0	1264.3
(1,0,1)	690.8	1296.1
	(v_s, v_b, v_a) $(0,0,0)$ $(0,0,1)$ $(0,0,2)$ $(0,2,0)$ $(0,0,3)$ $(0,2,1)$ $(0,0,4)$ $(0,2,2)$ $(0,2,3)$ $(0,0,5)$ $(1,0,0)$	

are more difficult to assign due to the extreme floppiness of the system. They tend to extend toward the dissociative channels, as can be seen in Figure 10 where the probability densities for states n=16 and 25 for the even parity and n=17 and 22 for the odd symmetry are represented as an example. It is interesting to note that they contain a relatively low vibrational excitation in the bending mode θ and the symmetric stretch ρ .

Note that the symmetric stretch excitation is slightly more than half of the first dissociation energy. This suggests that it may be possible to record the spectrum of this mode, and others that couple to it strongly, by infrared beam-depletion experiments.

Conclusions

We have determined all the bound vibrational levels of the He₂Ne⁺ complex using a previously published potential energy surface.⁷ The calculation was performed using a truncation—diagonalization method based on DVR basis functions in terms of Radau hyperspherical coordinates. We have found 52 bound levels, 27 even, and 25 odd parity. Only four of these states lie below the classical dissociation limit, the 48 other states being bound because of the zero-point energy of the HeNe⁺ fragment. The ground state lies about half way to dissociation, 605.3 cm⁻¹

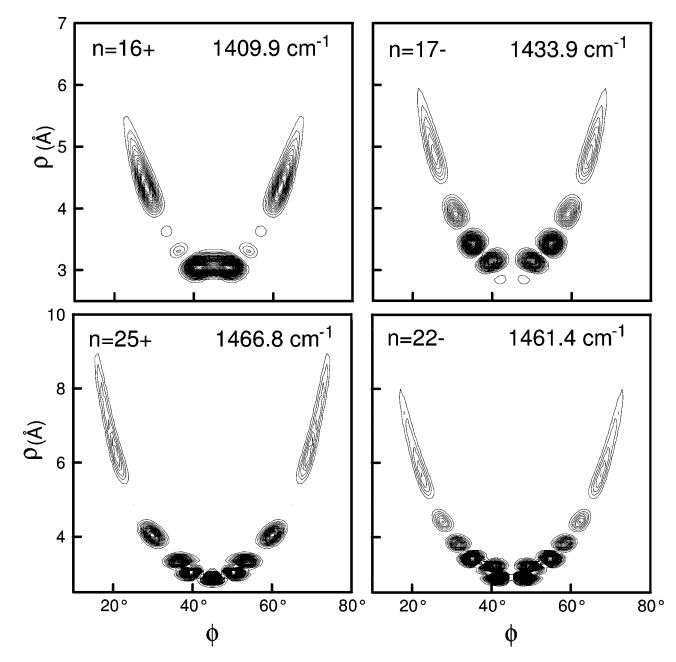


Figure 10. Contour plots of the probability density for the n=16 and 25 even and n=17 and 22 odd states of He_2Ne^+ in hyperspherical Radau coordinates at the colinear ($\theta=180^\circ$) geometry.

above the absolute minimum, and the energy necessary to dissociate one He atom has been determined to be 866.1 cm⁻¹.

There is a high density of levels near the threshold (14 levels within 25 cm⁻¹ of dissociation), and the corresponding wave functions extend over long bond distances. This is because of the long-range (charge-induced dipole) attractive interaction in this system. It is therefore expected that the odd parity states will show large dipole moments, making the infrared spectroscopy of these species feasible.³² The high density of states near dissociation and the wide amplitude vibrations of this system will make vibrational relaxation very efficient even at low temperatures. We conclude that the He₂Ne⁺ core is the most likely candidate for energy relaxation with the concomitant ejection of He atoms in the ionization of Ne atoms embedded in He clusters, once the charge has been localized on the Ne atom. This will be of significance to interpret and possibly predict the distribution of He_ND⁺ fragments in the electronimpact ionization of doped clusters.

The results presented in this work are converged to about 0.1 wavenumbers for the potential energy surface determined by Seong et al.⁷ The accuracy of the potential energy surface was discussed above and in ref 7. Results for the potential energy minimum were found to be quite sensitive to the basis set and the extent of correlation employed. However, the long-range parts of the potential are expected to be quite accurate since they are based on the best available potentials for the constituent diatomic interactions. Due to the high zero-point energy of the ground state, the details of the potential energy minimum are not expected to significantly influence the results presented here. The calculations reported here are for angular momentum equal to zero. While issues such as vibrational relaxation and cluster fragmentation are not expected to be very sensitive to rotational effects, the light mass of helium and the wide amplitude motions of the vibrational states imply that the rotational spectra of this ion will be quite interesting. Calculations for the rotational excited states are underway.

Acknowledgment. The work was partially supported by the Ministerio de Ciencia e Innovación of Spain under Project CTQ2007-66528/BQU, by the Fundación Séneca de Agencia Regional de Ciencia y Tecnología de la Región de Murcia (Spain) under Project 08735/PI/08 and by the CNRS through a PICS N ° 4648.

References and Notes

- (1) Lewerenz, M.; Schilling, B.; Toennies, J. P. J. Chem. Phys. 1995, 102, 8191–8207.
- (2) Callicoatt, B. E.; Förde, K.; Ruchti, T.; Jung, L.; Janda, K. C.; Halberstadt, N. *J. Chem. Phys.* **1998**, *108*, 9371.
- (3) Ruchti, T.; Förde, K.; Callicoatt, B. E.; Ludwigs, H.; Janda, K. C. *J. Chem. Phys.* **1998**, *109*, 10679–10687.
- (4) Ruchti, T.; Callicoatt, B. E.; Janda, K. C. *Phys. Chem. Chem. Phys.* **2000**, 2, 4075–4080.
- (5) Kim, J. H.; Peterka, D. S.; Wang, C. C.; Neumark, D. M. J. Chem. Phys. 2006, 124, 214301.
- (6) Murrell, J. N.; Naumkin, F. Y.; Griffiths, C. R. Mol. Phys. 2001, 99 115-132
- (7) Seong, J.; Rohrbacher, A.; Li, Z. R.; Janda, K. C.; Tao, F. M.; Spiegelman, F.; Halberstadt, N. J. Chem. Phys. **2004**, 120, 7456–7463.
- (8) Brindle, C. A.; Prado, M. R.; Janda, K. C.; Halberstadt, N.; Lewerenz, M. J. Chem. Phys. **2005**, 123, 064312.
- (9) Wright, T. G.; Gray, B. R.; Viehland, L. A.; Johnsen, R. J. Chem. Phys. 2008, 129, 184307.
- (10) Ragni, M.; Bitencourt, A.; Aquilanti, V. Hyperspherical and related types of coordinates for the dynamical treatment of three-body systems. In *Topics in the theory of chemical and physical systems*; Lahmar, S., Ed.; Springer: 2007; pp 123–146.
- (11) Ragni, M.; Bitencourt, A.; Aquilanti, V. Int. J. Quantum Chem. **2007**, 107, 2870–2888.
 - (12) Aquilanti, V.; Cavalli, S. J. Chem. Phys. 1986, 85, 1355-1361.

- (13) Aquilanti, V.; Cavalli, S.; Grossi, G. J. Chem. Phys. 1986, 85, 1362–1375.
- (14) Sun, X. Y.; Li, Z. R.; Wu, D.; Sun, C. C.; Gudowski, S.; Tao, F. M.; Janda, K. C. *J. Chem. Phys.* **2005**, *123*, 134304.
- (15) Skokov, S.; Qi, J.; Bowman, J. M.; Yang, C. Y.; Gray, S. K.; Peterson, K. A.; Mandelshtam, V. A. J. Chem. Phys. 1998, 109, 10273– 10283.
 - (16) Whitnell, R. M.; Light, J. C. J. Chem. Phys. 1989, 90, 1774.
 - (17) Choi, S. E.; Light, J. C. J. Chem. Phys. 1992, 97, 7031-7054.
- (18) Henderson, J. R.; Sueur, C. R. L.; Tennyson, J. Comput. Phys. Commun. 1993, 75, 379–395.
- (19) Bramley, M. J.; Carrington, T., Jr. J. Chem. Phys. 1994, 101, 8494– 8507
- (20) Bastida, A.; Zúñiga, J.; Requena, A.; Halberstadt, N.; Beswick, J. A. Faraday Discuss. 1994, 97, 131–142.
- (21) Dobbyn, A. J.; Stumpf, M.; Keller, H. M.; Schinke, R. *J. Chem. Phys.* **1995**, *103*, 9947–9962.
- (22) Mussa, H. Y.; Tennyson, J. J. Chem. Phys. 1998, 109, 10885–10892.

- (23) Zúñiga, J.; Bastida, A.; Requena, A.; Sibert, E. L. J. Chem. Phys. **2002**, 116, 7495–7508.
 - (24) Bacic, Z.; Light, J. C. Annu. Rev. Phys. Chem. 1989, 40, 469-498.
 - (25) Choi, S. E.; Light, J. C. J. Chem. Phys. 1990, 92, 2129–2145.
- (26) Tennyson, J.; Miller, S.; Henderson, J. R. Methods of Computational Chemistry; Wilson, S., Ed.; Plenum Press: New York, 1992; pp 91–144.
- (27) Zúñiga, J.; Bastida, A.; Requena, A. *J. Phys. Chem.* **1992**, *96*, 4341–4346.
- (28) Requena, A.; Bastida, A.; Zúñiga, J. Chem. Phys. **1993**, 175, 255–264.
 - (29) Smith, F. T. Phys. Rev. Lett. 1980, 45, 1157.
- (30) Johnson, B. R.; Reinhardt, W. P. J. Chem. Phys. 1986, 85, 4538–4556
- (31) Seong, J.; Janda, K. C.; McGrath, M. P.; Halberstadt, N. Chem. Phys. Lett. 1999, 314, 501–507.
- (32) Cox, S. G.; Critchley, A. D. J.; McNab, I. R.; Smith, F. E. Meas. Sci. Technol. 1999, 10, R101.

JP905043T